Bayesian Analysis of Microfluidic Particle and Cluster Sorting

Elham Akbari , Esra Yilmaz , Christelle N. Prinz , Jason P. Beech , Jonas O. Tegenfeldt *

Posted Date: 26 February 2026

doi: 10.20944/preprints202602.1312.v1

Keywords: deterministic lateral displacement; microfluidics; sorting; Bayesian statistics

Article

Bayesian Analysis of Microfluidic Particle and Cluster Sorting

Elham Akbari †, Esra Yilmaz †, Christelle N. Prinz, Jason P. Beech and Jonas O. Tegenfeldt *

Department of Physics, Division of Solid State Physics, Lund University, Lund, Sweden
* Correspondence: jonas.tegenfeldt@fysik.lu.se
† These authors contributed equally to this work.

Abstract

Deterministic lateral displacement (DLD) and related microfluidic sorting devices are typically evaluated based on the size distributions of particles collected at each outlet, even though the more relevant measure of performance is the probability that a particle of a given size ends up in a specific outlet. Here, we introduce a Bayesian framework that infers these size-dependent routing probabilities from experimentally accessible measurements of outlet size distributions, inlet size distributions, and outlet fractions. Using a DLD array designed to separate microspheres and microsphere clusters, we determine the probabilities that particles of different sizes are directed to each outlet and define a probabilistic critical size (D_c) at which particles are equally likely to follow zigzag or displacement trajectory. From these routing probabilities, we calculate key performance metrics, purity and yield. Our results demonstrate high-quality separations and show that routing probabilities provide a general and robust framework for benchmarking microfluidic sorting devices beyond traditional outlet-based analyses.

Keywords: deterministic lateral displacement; microfluidics; sorting; Bayesian statistics

1. Introduction

A common theme in microfluidic sorting devices is that the unsorted sample is introduced in one end of a long channel and exits into several outlet reservoirs at the end of the channel. Examples include inertial focusing [1], viscoelastic focusing [2], pinched flow fractionation [3] and deterministic lateral displacement (DLD) [4]. To assess the performance of these types of devices, different approaches are employed. The performance of a sorting device is multifaceted and must be described using a broad range of performance indicators depending on the application at hand [5]. Throughput is essential for preparative applications. It can be related to inlet and outlets volumes, number of cells processed, number of cells produced, time to answer. Purity is essential for some preparative applications such a cell therapy where no contamination is allowed [6]. The definition of purity varies with whatever goals are on the table. To start with, one can consider a device-centric definition such that for a device with cut-offs that define a subpopulation, purity is simply the number of cells within the cut-off range divided by all cell. As an alternative, one can consider a goal-oriented definition that is defined on the needs of the application at hand. In this case purity is simply the number of desired cells divided by the total number of cells. Capture rate (or yield) is important for rare cells as is enrichment ratio [7]. Resolution can be quantified by the overlap of the two routing probabilities.

In the most common situations, the compositions in the outlets are known, i.e. the probability distribution of sizes within an outlet, $P(size|outlet)$. However, to evaluate the separation performance, what is really needed is the probability $P(outlet|size)$ of a particle of a given size to end up in a specific outlet, i.e. among all particles of a given size, what fraction goes to respective outlet. We call these probabilities the routing probabilities.

In our study, we use data from sorting devices based on DLD. It is a method that is based on the flow of particles through a regular array of posts. The particles ideally follow one out of two

 doi:10.20944/preprints202602.1312.v1

distinct trajectories. Particles with a diameter less than a critical diameter, ($D < D_c$) , follow the flow through the device, in the zigzag mode, while particles with diameters greater than the critical diameter, ($D > D_c$) , follow a direction determined by the orientation of the array, in the displacement model [4].

The array in turn can be defined in one out of two major ways. From a design perspective it is more straightforward to use a square array that is rotated slightly within the flow channel. For simulations, and for devices based on multiple sequential DLD arrays with different D_c , the rhombic array is more convenient [8]. To estimate the critical size, a simple expression can be used that is an approximation of an empirical expression reported by Davis [9]. The approximate expression is $D_C = G\sqrt{(2/N)}$, where G is the gap between the posts and N is the periodicity of the DLD array. The periodicity is related to the orientation angle of the array as follows: $tan\theta = 1/N$.

While the simple picture of a DLD device comprises a binary and deterministic sorting mechanism, real devices are more complex making it difficult to identify a sharp threshold size. This is due to inherent properties of the DLD design in itself as well as due to the complexity of relevant particles. For small particles, diffusion makes the transition between zig and displacement mode gradual [4,10,11]. For array periodicities that are not integers, anomalous trajectories can appear [10]. Specifically for rhombic arrays, anisotropic permeability of the array results in a broadening of the transition between zig and displacement modes [12–14]. This is predicted to happen also for square arrays for high Reynolds numbers, but not for low Reynolds numbers [15]. Finally boundary effects, such as wall effects, can be significant, especially for narrow devices [16]. These can be compensated for by careful design of the structure of the walls [17].

Many relevant biological samples are not spherical hard particles. Their shape and deformability will affect the way they move through the DLD array in ways that are often difficult to predict using a simple equation [18–21]. Some shapes leads to chaotic motion, and if particles aggregate, they can change shape dynamically as they move through the device. Particle-particle interactions is another mechanism that is highly relevant for undiluted samples. Separating particles in blood, the effective D_c shifts and the dispersion of the particle trajectories increase with increasing hematocrit [22].

Together, all this creates an urgent need for a well-defined scheme of characterizing key performance indicators for different types of samples that are handled in DLD devices.

In our recent work, we demonstrated the sorting of bacterial clusters with a broad size distribution using a high-N DLD device. We have shown that introducing an intermediate outlet between the displacement and zigzag outlets increases purity by collecting particles that exhibit significant dispersion due to their broad variation in shape and sizes near the device's critical diameter [23]. For such complex samples, we showed that the device's effective critical diameter, D_c, can be determined using routing probabilities. Building on this approach, we now calculate the routing probabilities of single microspheres and microsphere clusters to evaluate the device performance when sorting particles with well-defined and controlled properties.

Here, routing probability refers to the conditional probability, $P(outlet|size)$, which in turn is understood as: given a size of the particle, what are the probabilities that it ends up in each of the outlets. The challenge is that it is difficult to directly measure $P(outlet|size)$. Instead, we can readily measure the size distributions in each outlet, $P(size|outlet)$, along with the size distribution of the unsorted particles, $P(size)$, and the fraction of all particles that end up in each outlet $P(outlet)$. We then use Bayesian statistics to calculate $P(outlet|size)$ for a DLD device designed to separate microspheres and microsphere clusters based on size.

We show that using routing probabilities, we can expand the traditional definition of the critical size, D_c, from a threshold size separating two adjacent binary distributions, to a quantitative border between two overlapping outlet distributions. We thus define the D_c as the size for which the routing probabilities are equal:

$P(outlet1|size = DC) = P(outlet2|size = DC)$ Note that this critical diameter is related to but not identical to the D_c typically associated with DLD devices [4,24].

 doi:10.20944/preprints202602.1312.v1

Once we have the routing probabilities along with the measured size distributions we calculate the various performance indicators, such as purity and yield. Purity corresponds to the fraction of desired particles to the total number of particles in an outlet. Yield is defined as the fraction of particles in the inlet in the desired size range that are sent to the desired outlet.

2. Materials and Methods

In this chapter, we describe the particles employed, the device fabrication process, data acquisition, and data analysis.

2.1. Microspheres

Microspheres were purchased from Duke Scientific, with the following properties:

Table 1. Microspheres used in the experiments.

Color	Diameter (μm)	Coefficient of variation (CV%)	Lot Number
Green	7	13%	26920
Red	10	12%	27150
Green	16	12%	27640

Microspheres were diluted by a factor of 100X in a Pluronic(MW 12,500 Da) 0.5% w/v water solution to minimize aggregation and clogging in the devices and were run in 2 sets of experiments (7 μm and 10 μm microspheres together and 16 μm in another experiment). The 7μm and 16μm particles share the same excitation wavelength; therefore, they were tested in separate experiments to avoid mixing in the observation area where the normalized intensity was measured (Figure 2). All experiments were performed 3 times and the data was pooled together.

2.2. DLD Device Design

We tested the routing probability analysis on DLD device used in our earlier study for bacteria clusters sorting [23]. The device features one rotated square array with a high periodicity (N=69). The rotated square array was made of circular pillars of diameter D = 50 μm, with a gap between pillars G = 45 μm (λ=D+G=95 μm), a tilt angle with respect to the flow direction θ = 0.83° which gives a critical diameter $D_c \approx 8$ μm calculated based on Davis equation [9].

The device has two inlets, three outlets (zigzag, intermediate and displacement outlets), and an observation area where the flow velocity is 10 times lower than in the rest of the device (Figure 1). The observation area is placed to track particles' lateral positions after being sorted by the DLD array and before collection in the outlets. This is used to assure a stable flow throughout the device during the experiment.

 doi:10.20944/preprints202602.1312.v1

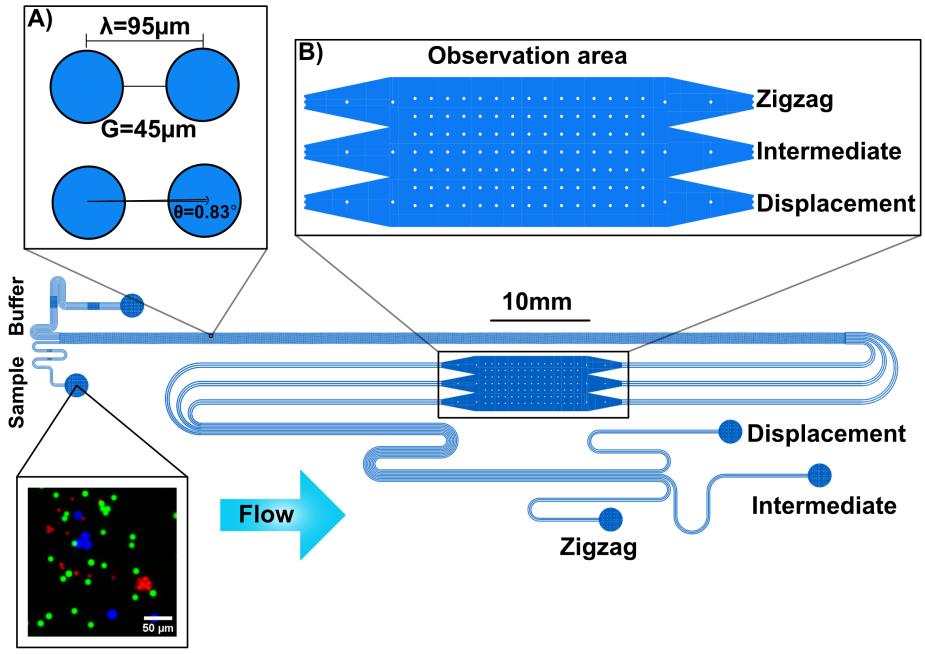

Figure 1. Schematic of the DLD device used in this study. A) Key dimensions in the rotated square array device. The device has two inlets (buffer and sample inlet), an observation area and three outlets (Zigzag, intermediate and displacement). Particles smaller than D_c move in zigzag mode and exit the device via the Zigzag outlet. particles larger than D_c move in the displacement mode and are collected in the Displacement outlet. If there are any other moving not in displacement nor zigzag, they are expected to collect in the intermediate outlet. B) The device also contains an observation area, used to observe the lateral particle distributions at the end of the array and before collection in the outlets

The inlets consist of one sample inlet and one buffer inlet. The buffer inlet consists of seven parallel channels, and the sample inlet consists of three parallel channels, each of 50 μm in width. With equal flow speed between sample and buffer at the entrance of the DLD device, the sample is diluted to 30% of its concentration in the sample inlet.

The buffer and sample inlet channels have equal fluidic resistances per unit width and the same applies to the three outlet channels. However, the outlet channels are longer than the inlet channels, which increases their resistance, which we found helps stabilize the flow. By balancing the resistances at the inlets and outlets, the flow is guided to enter and exit the array in the same direction, remaining parallel to the side walls.

DLD Device Fabrication

A master mold was prepared using 100-μm-thick SUEX® dry film resist (K100, DJ Microlaminates, Sudbury, MA, USA), which was laminated onto a 4 inch silicon wafer with a laminator (Catena 35, Acco UK Ltd, Buckinghamshire, UK) at 65 °C. The laminated wafer was then baked on a hotplate (Model 1000-1 Precision Hot Plate, Electronic Micro Systems Ltd, West Midlands, UK) at 85 °C for 5 min to eliminate trapped air and allow the resist to relax. The channel layout was patterned onto the resist using a photomask (Delta Mask B.V., Enschede, The Netherlands). UV exposure was performed at 365 nm in a contact mask aligner (Karl Suss MJB4 Soft UV, Munich, Germany) for 34 s with a lamp intensity of 30 mW/cm^2, followed by a post-exposure bake at 85 °C for 5 min. Development of the exposed SU-8 was carried out in mr-DEV 600 (Micro Resist Technology GmbH, Berlin, Germany) for 15 min, followed by an additional 5 min in fresh developer. The mold was then rinsed in flowing IPA and dried under nitrogen to remove any unpolymerized resist.

A final hard bake at 200 °C for 2 h in a convection oven completed the master. To avoid PDMS sticking during replica molding, the surface was coated with a 1-nm aluminium oxide layer and

 doi:10.20944/preprints202602.1312.v1

subsequently functionalized with a Perfluorodecyltrichloro-silane (FDTS) monolayer using a Fiji Plasma-Enhanced ALD system (Veeco, NY, USA).

The PDMS devices were fabricated from this master by standard replica molding following the method of Xia et al. [24] PDMS (Sylgard 184, Dow Corning, Midland, MI, USA) was cast, cured, and then peeled from the master. Inlet and outlet holes were punched prior to bonding. Oxygen-plasma activation (Zepto, Diener electronic GmbH & Co. KG, Ebhausen, Germany) was applied for 15 s to the PDMS and 50 s to the glass substrates, after which the two surfaces were brought into contact to seal the channels. Immediately after bonding, the channels were filled with poly(acrylamide)-g-(PMOXA, 1,6-hexanediamine, 3-aminopropyldimethylsilanol) (PAcrAm-g-(PMOXA, NH_2, Si)) (SuSoS AG, Dübendorf, Switzerland).

2.3. Fluidics and Sample Handling

Flow through the device was established by leaving the outlets at atmospheric pressure while supplying nitrogen overpressure to the inlets. These pressures were finely tuned to produce a uniform, stable flow along the pillar array. The sample and buffer were pressurized in two 15 mL tubes using an MFCS-4C controller (Fluigent, Paris, France), set to 140 mbar and 150 mbar, respectively. Under these conditions, the flow rate was $30 \pm 2\,\mu$L/min, giving an average shear rate of $210\,s^{-1}$ and, assuming water-like viscosity, a shear stress of approximately 0.2 Pa. This falls within commonly used ranges for biofilm experiments, physiological airway shear, and microfluidic perfusion systems [25].

The fluids were delivered to the device through capillaries with a 768 μm inner diameter. Before introducing samples, the channels were conditioned by flushing with running buffer (0.5% w/v pluronics) for 10 min.

2.3.1. Imaging and Analysis

All experiments were performed under observation using an inverted epifluorescence microscope (Nikon Eclipse TE2000-U, Nikon Corporation, Tokyo, Japan) in transmission mode with an EMCCD camera (Andor iXon, Andor Technology, Belfast, Northern Ireland). The following objectives were used: 10× Nikon Plan Apo λ, NA 0.45, field of view (FoV) of 819 μm; 20× Nikon Plan Fluor, NA 0.45, FoV of 320 μm; and 4× Nikon Plan Apo λ, NA 0.2, FoV of 25 mm. Imaging was performed using FITC and Cy5 filter cubes and an LED light source (Sola light engine, Lumencore, Beaverton, Oregon, USA).

For the separation experiments, batches of microscopic images from the inlet and outlet reservoirs were processed using a custom automated image-analysis workflow. In addition to basic segmentation and object characterization, the workflow incorporated normalization by the fluorescent lamp profile, background subtraction, compensation for spectral crosstalk between fluorescence channels, and identification of overlapping objects.

The pipeline was implemented in Python (Spyder/Anaconda 4) using packages including `numpy`, `matplotlib`, `skimage` (particularly `skimage.measure` with `RegionProps`), `cv2`, `scipy`, and `pandas`, and Meta Segment Anything Model 2 (SAM 2) [26].

2.3.2. Microsphere Characterization in the Various Reservoirs

All separation experiments were performed 3 times, and the data were pooled. For microsphere and microsphere-cluster characterization, the 7 μm and 10 μm microspheres were imaged with a 20× objective (Nikon Plan Fluor, NA 0.45, FoV 320 μm), while the 16 μm microspheres were imaged with a 10× objective (Nikon Plan Apo λ, NA 0.45, FoV 819 μm).

The particles were imaged directly in the three outlets, each containing 300 μL of microsphere suspension. For characterization of the sample inlet, 10 μL of the solution was pipetted onto a glass slide, covered with a coverslip, and imaged. Taking into account dilution by the buffer, which reduced the sample concentration to 30% of its initial value at the device entrance, capture rates were evaluated for each nominal diameter population as the sum of the concentrations in the three outlets divided by 30% of the concentration in the sample inlet.

 doi:10.20944/preprints202602.1312.v1

For the 7 μm microspheres, 1680 particles were segmented and measured in the zigzag outlet and 1420 in the intermediate outlet. For the 10 μm microspheres, 1005 beads were measured in the zigzag outlet, 2500 in the intermediate outlet, and 1660 in the displacement outlet. For the 16 μm microspheres, 1140 beads were measured in the intermediate outlet and 3900 in the displacement outlet.

The uncertainty in particle counting was estimated to be 10-20%, primarily due to sedimentation in the reservoirs and tubing. Additional losses were attributed to clogging inside the device.

3. Results and Discussion

3.1. Sorting Result

The ability of the device to separate microspheres was evaluated for each microsphere diameter. The lateral positions of the particles were measured as they flowed through the observation area, and the microspheres were counted in the three outlet reservoirs. Figure 2 shows superposed, time-averaged, false-coloured fluorescence micrographs of the microspheres in the observation area. The background signal was subtracted, and each colour corresponds to a specific microsphere diameter. Note that the data include both singlets, and clusters of microsphere formed during long-term storage in the vials.

The normalized signal intensities of the microspheres as a function of their lateral position in the observation area are shown on the right-hand side of the fluorescence image in Figure 2.

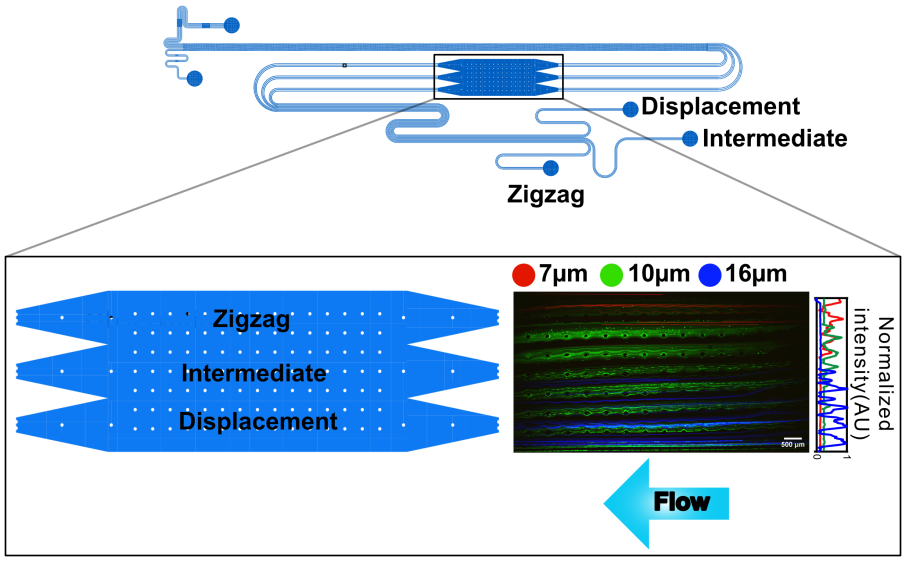

Figure 2. Final lateral position of the different microspheres inside the device's observation area. Schematic of the device mapping the observation area and positions where fluorescent intensities are measured. Close-up view of the observation area (schematics and fluorescence image) with the microspheres moving towards the zigzag outlet (Zigzag), the intermediate outlet (Intermediate), and the displacement outlet (Displacement). The fluorescence image were created using a maximum intensity projection and normalized signal intensity (2× magnification). The data are overlays from separate experiments, false-colored to enable diameter distinction (red: 7 μm, green: 10 μm, blue: 16 μm).

The distribution of microspheres Within the width of the observation area shows a separation of the particles by the DLD arrays. Majority of the 7μm beads exit through the zigzag, while almost all 16μm micospheres exist through the displacement region. 10μm micrpspheres with a size distribution close to device's D_c exits through the intermediate, and zigzag path.

After separation, for each nominal diameter, image analysis was performed to measure the size distributions of particles present in both the unsorted inlet population and the separated fractions collected in the three device outlets (Figure 3). Details on image analysis can be found in appendix. For single microspheres, the major axis corresponds to the microsphere diameter.

 doi:10.20944/preprints202602.1312.v1

Based on the presented data in boxplot and histogram plot in Figure 3-B, and C, the zigzag outlet contained only single 7 μm and 10 μm microspheres. The intermediate outlet contained single 7 μm and 10 μm microspheres, as well as small clusters (primarily pairs) of 7 μm microspheres. The displacement outlet contained both single particles of 16 μm microspheres and clusters of 7μm and 10μm.

The capture rate of the device was estimated for all three microsphere populations, and we found that most microspheres entering the device were recovered in the outlets (Table S1). Table S1 also shows the fraction of each microsphere type collected in each outlet. The 7 μm and 16 μm microspheres were separated into two fractions, above and below the nominal critical size D_c, whereas the 10 μm microspheres were found in zigzag, and intermediate outlets. This indicates that the actual critical size of the device lies within the size distribution of the 10 μm particles.

These results demonstrate the ability of the device to separate microspheres and microsphere clusters.

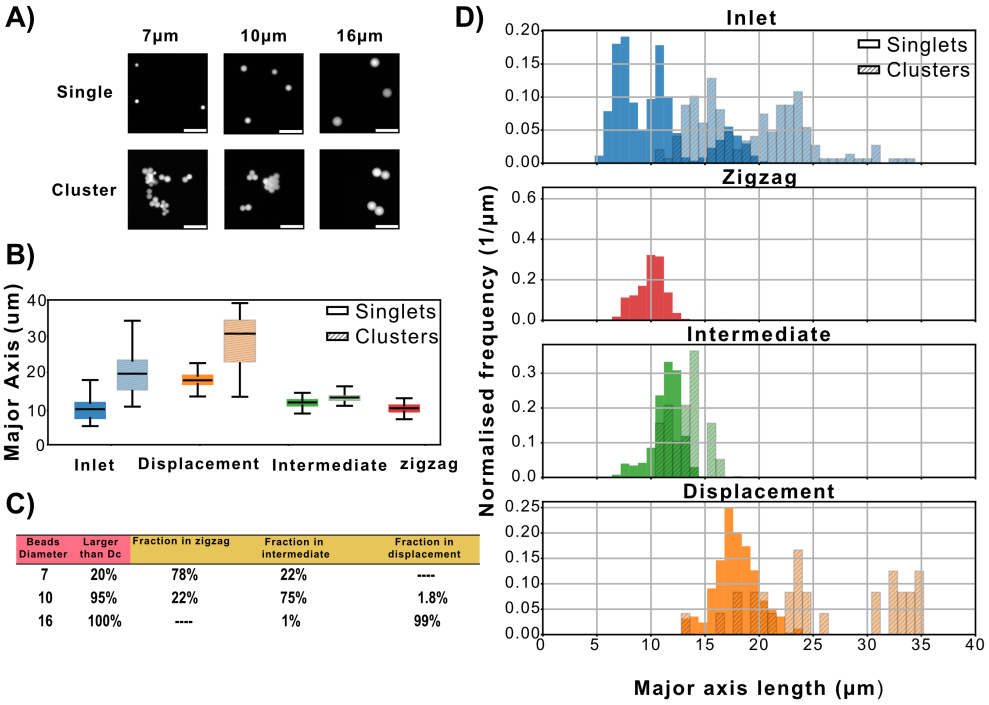

Beads Diameter	Larger than Dc	Fraction in zigzag	Fraction in intermediate	Fraction in displacement
7	20%	78%	22%	----
10	95%	22%	75%	1.8%
16	100%	----	1%	99%

Figure 3. Inlet composition and outlet content after separation of microspheres in the device. A) Representative fluorescence images of single microspheres and clusters of nominal diameter 7, 10 and 16 μm. Scale bars 30 μm. B) Boxplot of the major axis length of the microspheres and microspheres clusters present in each reservoir. The box shows the 25th, 50th and 75th percentile, the whiskers show the upper and lower limits. Note that for the spherical single beads, the major axis corresponds to the diameter. C) Fraction of sorted microspheres in each outlet for each nominal diameter population. The second column shows the percentage of particles larger than the nominal DC $\approx 8\mu$m in the inlet before separation, as measured using fluorescence microscopy. Columns 3-5 show the total fraction of microspheres and clusters of each nominal diameter found in each the outlets. D) Histogram of size values of the microspheres in the inlet and the three outlets. The histogram shows the normalized counts.

3.2. Bayes Analysis

To further characterize the sorting behavior of the DLD device, we used frequentist Bayesian statistics to estimate the routing probabilities of particles (singles and clusters) passing through the device. Because this method is applicable to other microfluidic sorting devices (not only DLD), we adopted more general terminology for the reservoirs: the inlet, the small outlet (corresponding to the DLD zigzag outlet), the medium outlet (corresponding to the DLD intermediate outlet), and the large outlet (corresponding to the DLD displacement outlet). The routing probabilities correspond to the probabilities $P(k \mid d_i)$ that a particle of size d_i from the inlet is routed to outlet $k \in \{S, M, L\}$ (Small, Medium, Large). For the size d_i, we used the major axis length, which, in the case of a perfect circle, corresponds to the diameter. Our starting point is the observed probability distributions of particle

 doi:10.20944/preprints202602.1312.v1

sizes in the sample inlet (I) and in the three outlets $\{S, M, L\}$. We used the convention of conditional probabilities to refer to subsets belonging to a total set of data points. These are summarized in Table S2 and illustrated in Figure S2.

We derive the routing probabilities for different particle sizes step by step to make it clear where assumptions and simplifications are introduced.

Step 1: We assume that there is no loss in the device and that all particles move from the inlet to the outlets. The probability $P(k \mid d_i)$ that a particle of size d_i finds its way from the inlet to outlet k is given by the total number of particles $n_{d_i,k}$ of size d_i present in outlet k, divided by the total number of particles of size d_i across all outlets.

$$P(k \mid d_i) = \frac{n_{d_i,k}}{\sum_{j\in\{S,M,L\}} n_{d_i,j}}, \quad k \in \{S, M, L\} \tag{1}$$

Step 2: The total number of particles nd_i, k of size d_i that exist in outlet k, is given by the total number of particles n_k in outlet k, multiplied by the fraction $P(d_i|k)$ of particles of size d_i in outlet k:

$$P(k \mid d_i) = \frac{n_k\, P(d_i \mid k)}{\sum_{j\in\{S,M,L\}} n_j\, P(d_i \mid j)}, \quad k \in \{S, M, L\} \tag{2}$$

Step 3: The total number of particles n_k that exist in outlet k is given by the total number of particles in the device (initially added to the inlet) N, multiplied by the fraction $P(k)$ of all particles that end up in outlet k:

$$P(k \mid d_i) = \frac{N\, P(k)\, P(d_i \mid k)}{\sum_{j\in\{S,M,L\}} N\, P(j)\, P(d_i \mid j)}, \quad k \in \{S, M, L\} \tag{3}$$

Step 4: We note that the total number of particles N in the device cancels out. We also note that the denominator equals the normalized size distribution of the entire set of particles $P(d_i)$.

$$P(k \mid d_i) = \frac{P(k)\, P(d_i \mid k)}{P(d_i)}, \quad k \in \{S, M, L\} \tag{4}$$

Assuming that all particles are distributed equally among the outlets, we have $P(S) = P(M) = P(L) = 1/3$, i.e. they all cancel-out and we have instead:

$$P(k \mid d_i) = \frac{P(d_i \mid k)}{3\, P(d_i)}, \quad k \in \{S, M, L\} \tag{5}$$

The routing probabilities for the DLD device are plotted in Figure 4.

The particle size (major axis length) at which the probability of ending up in the small (zigzag) outlet equals the probability of ending up in the large (displacement) outlet can be interpreted as the effective critical diameter for the corresponding sample and device ($\approx 12\,\mu$m). The particles collected in the intermediate outlet can be regarded as a trade-off, representing a loss that enables higher purity in the small and large subpopulations.

 doi:10.20944/preprints202602.1312.v1

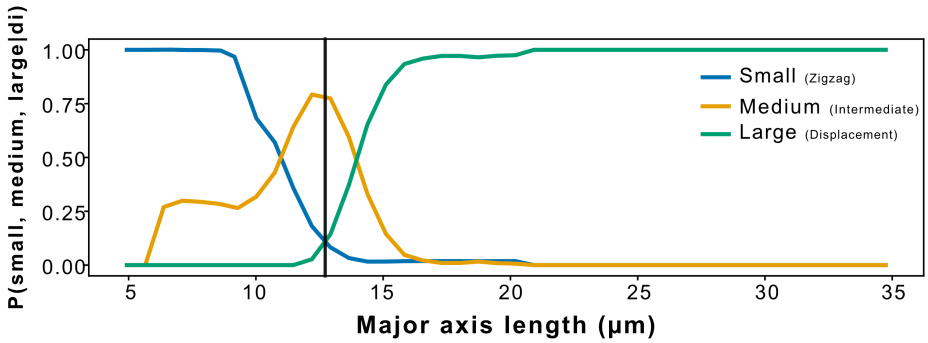

Figure 4. Routing probabilities $P(S|di)$, $P(M|di)$, $P(L|di)$ to the three outlets of singlets and clusters of microspheres of different size. The crossover for the zigzag and displacement outlets gives the D_c 12 μm with a negligible overlap between the two fractions.

We then used the measured size distributions of singlets and clusters of microspheres in each outlet together with the calculated routing probabilities to determine the purity and yield of the sorting process.

We define the purity of a subpopulation in a reservoir as the number of particles in the desired size range divided by the total number of particles in that reservoir. The purity of the Small outlet (zigzag) subpopulation, Purity(S), is defined as the fraction of particles in that outlet having a diameter smaller than the critical diameter D_c. This is obtained by summing the elements of the size probability distribution in the outlet, $P(d_i \mid k)$, from the minimum size (corresponding to $i = 1$) up to D_c:

$$\text{Purity}(S) = P(d < D_c \mid S). \tag{S6}$$

Similarly, the purity of the Large outlet (displacement) subpopulation is defined as

$$\text{Purity}(L) = P(d > D_c \mid L). \tag{S7}$$

The yield of a subpopulation in an outlet reservoir is defined as the fraction of particles in the inlet, within the desired size range, that are routed to the desired outlet.

The yield of the Small outlet subpopulation is defined as the fraction of inlet particles with diameter smaller than the critical diameter D_c that are routed to the Small outlet. This is obtained by summing the routing probability distribution $P(S \mid d_i)$ from the minimum size up to D_c:

$$\text{Yield}(S) = P(S \mid d < D_c). \tag{S8}$$

Similarly, the yield of the Large outlet subpopulation is defined as

$$\text{Yield}(L) = P(L \mid d > D_c). \tag{S9}$$

Due to the difficulty of precisely estimating the fraction of the sample entering the device, we report the yield as a nominal yield, assuming that the total number of particles collected in all outlets equals the total number entering from the inlet. This assumption is supported by the low loss reported in Table S1. However, the reported yield does not provide precise information regarding any selective losses between the inlet and outlet reservoirs.

From the measured size distributions in the reservoirs (Figure3) and the routing probabilities (Figure 4), we calculated a purity of 96% for the small fraction and 100% for the large fraction, with corresponding yields of 73% and 94%, respectively. These values indicate adequate sorting performance. The microspheres ending up in the intermediate outlet can be regarded as a necessary trade-off to achieve higher purity in the small and large subpopulations.

 doi:10.20944/preprints202602.1312.v1

4. Conclusions

In this study, we have demonstrated that routing probabilities provide a rigorous and versatile framework for characterizing the performance of DLD devices. By inferring the probability that a particle of a given size reaches each outlet from experimentally measurable size distributions, we capture the complex effects of diffusion, array geometry, and interactions that challenge idealized deterministic models. This approach allows us to define a probabilistic critical size and to calculate key performance metrics. The results highlight that even in the presence of real-world complexities, DLD devices can achieve high-quality separations. More broadly, routing probabilities offer a generalizable method for benchmarking microfluidic sorting systems and can guide the rational design and optimization of devices for diverse applications, from synthetic particle separation to complex biological samples.

Supplementary Materials: The following supporting information can be downloaded at the website of this paper posted on Preprints.org.

Author Contributions: Conceptualization, E.A., E.Y, J.P.B and J.O.T.; Data collection, E.A., E.Y, J.P.B; Formal Analysis, E.A.; Funding Acquisition, J.O.T.; Investigation, E.A., E.Y., J.P.B and J.O.T.; Methodology, E.A., E.Y., J.P.B and J.O.T.; Project Administration, J.O.T.; Resources, J.O.T.; Software, E.A.; Supervision, C.P., J.P.B., and J.O.T.; Validation, E.A., J.P.B and J.O.T.; Visualization, E.A.; Writing - Original Draft, C.P., E.A., E.Y.; Writing - Reviewing & Editing, E.A., E.Y., C.P., J.P.B, and J.O.T.

Acknowledgments: We acknowledge financial support by the Swedish Research Council (grants number 2019-02355 and 2019-04102), and from NanoLund (grants number p20-2019, s01-2024, and staff01-2020) and the Crafoord foundation. All device fabrication took place in the cleanroom of Lund Nano Lab at Lund University.

Conflicts of Interest: The authors declare no conflict of interest.

References

1. Di Carlo, D.; Irimia, D.; Tompkins, R.G.; Toner, M. *Proceedings of the National Academy of Sciences of the United States of America* **2007**, *104*, 18892–18897.
2. Liu, P.; Liu, H.; Semenec, L.; Yuan, D.; Yan, S.; Cain, A.K.; Li, M. *Microsystems & Nanoengineering* **2022**, *8*, 7.
3. Takagi, J.; Yamada, M.; Yasuda, M.; Seki, M. *Lab on a Chip* **2005**, *5*, 778–784.
4. Huang, L.R.; Cox, E.C.; Austin, R.H.; Sturm, J.C. *Science* **2004**, *304*, 987–990.
5. Gossett, D.R.; Weaver, W.M.; Mach, A.J.; Hur, S.C.; Tse, H.T.K.; Lee, W.; Amini, H.; Di Carlo, D. *Analytical and Bioanalytical Chemistry* **2010**, *397*, 3249–3267.
6. Zhang, T.; Di Carlo, D.; Lim, C.T.; Zhou, T.; Tian, G.; Tang, T.; Shen, A.Q.; Li, W.; Li, M.; Yang, Y.; et al. Passive microfluidic devices for cell separation. *Biotechnology Advances* **2024**, *71*, 108317.
7. Witek, M.A.; Freed, I.M.; Soper, S.A. Cell separations and sorting. *Analytical chemistry* **2019**, *92*, 105–131.
8. Salafi, T.; Zhang, Y.; Zhang, Y. A review on deterministic lateral displacement for particle separation and detection. *Nano-Micro Letters* **2019**, *11*, 77.
9. Davis, J.A. Microfluidic Separation of Blood Components through Deterministic Lateral Displacement. PhD thesis, Princeton University, 2008.
10. Long, B.R.; Heller, M.; Beech, J.P.; Linke, H.; Bruus, H.; Tegenfeldt, J.O. *Physical Review E* **2008**, *78*.
11. Heller, M.; Bruus, H. *Journal of Micromechanics and Microengineering* **2008**, *18*.
12. Kulrattanarak, T.; van der Sman, R.G.M.; Schroën, C.G.P.H.; Boom, R.M. *Microfluidics and Nanofluidics* **2011**, *10*, 843–853.
13. Kim, S.C.; Wunsch, B.H.; Hu, H.; Smith, J.T.; Austin, R.H.; Stolovitzky, G. *Proceedings of the National Academy of Sciences* **2017**, *114*, E5034.
14. Vernekar, R.; Kruger, T.; Loutherback, K.; Morton, K.; Inglis, D.W. *Lab on a Chip* **2017**, *17*, 3318–3330.
15. Mallorie, C.; Vernekar, R.; Owen, B.; Inglis, D.W.; Krüger, T. *Physical Review Fluids* **2024**, *9*, 024203.
16. Pariset, E.; Pudda, C.; Boizot, F.; Verplanck, N.; Berthier, J.; Thuaire, A.; Agache, V. *Small* **2017**, *13*, 11.
17. Inglis, D.W. *Applied Physics Letters* **2009**, *94*.
18. Holm, S.H.; Beech, J.P.; Barrett, M.P.; Tegenfeldt, J.O. *Analytical Methods* **2016**, *8*, 3291–3300.
19. Henry, E.; Holm, S.H.; Zhang, Z.M.; Beech, J.P.; Tegenfeldt, J.O.; Fedosov, D.A.; Gompper, G. *Scientific Reports* **2016**, *6*.
20. Beech, J.P.; Holm, S.H.; Adolfsson, K.; Tegenfeldt, J.O. *Lab on a Chip* **2012**, *12*, 1048–1051.

 doi:10.20944/preprints202602.1312.v1

21. Holm, S.H.; Beech, J.P.; Barrett, M.P.; Tegenfeldt, J.O. *Lab on a Chip* **2011**, *11*, 1326–1332.
22. Holm, S.H.; Zhang, Z.M.; Beech, J.P.; Gompper, G.; Fedosov, D.A.; Tegenfeldt, J.O. *Physical Review Applied* **2019**, *12*.
23. Akbari, E.; Beech, J.P.; Ahnlide, J.K.; Wrighton, S.; Nordenfelt, P.; Tegenfeldt, J.O. Size-based sorting of dynamic bacterial clusters. *Lab on a Chip* **2026**.
24. Xia, Y.N.; McClelland, J.J.; Gupta, R.; Qin, D.; Zhao, X.M.; Sohn, L.L.; Celotta, R.J.; Whitesides, G.M. *Advanced Materials* **1997**, *9*, 147–149.
25. Kim, L.; Toh, Y.C.; Voldman, J.; Yu, H. *Lab on a Chip* **2007**, *7*, 681–694.
26. Kirillov, A.; Mintun, E.; Ravi, N.; Mao, H.; Rolland, C.; Gustafson, L.; Xiao, T.; Whitehead, S.; Berg, A.C.; Lo, W.Y.; et al. Segment anything. In Proceedings of the Proceedings of the IEEE/CVF international conference on computer vision, 2023, pp. 4015–4026.